




Biochar from Al(OH)₃-activated sugarcane bagasse for efficient removal of cadmium: Optimization using the response surface method (RSM)

Mahmoud M. A. Bakr^{1,2,3} · Yongtai Wang^{1,2} · Peng Hao² · M. M. A. Dawoud⁴ · Liangcai Peng^{1,2} · Yanting Wang^{1,2} 

Received: 19 October 2024 / Revised: 10 January 2025 / Accepted: 26 January 2025
© The Author(s), under exclusive licence to Springer-Verlag GmbH Germany, part of Springer Nature 2025

Abstract

Biochar has been widely recognized as an environmentally efficient adsorbent for removing heavy metals in wastewater. In this study, an Al(OH)₃-modified sugarcane bagasse biochar (MSCB) was first prepared under slow pyrolysis at 350 °C to enhance the removal efficiency of cadmium (Cd²⁺) from aqueous solution. Fourier-transform infrared spectroscopy (FTIR), X-ray diffraction (XRD), scanning electron microscopy/energy-dispersive X-ray spectroscopy (SEM–EDX), and Brunauer–Emmett–Teller surfaces (BET) were used to interpret the characteristics of the biochar. The Box–Behnken design (BBD) was utilized to define the optimum conditions, including pH, Cd²⁺ concentration, and time of each experimental run-through response surface methodology (RSM). ANOVA analysis indicated a strong positive correlation and the estimated correlation coefficient values (R^2 0.9069) closely aligned with the adjusted value (R^2 0.9865), providing strong evidence of a highly significant model for Cd²⁺ adsorption. Additionally, the applicability of this model was assessed using the F-test (131.27) with a correspondingly low probability value (0.0001). The adsorption data better fitted the pseudo-second-order kinetic model and Langmuir isotherm model suggested a chemisorption mechanism. The optimum Cd²⁺ adsorption of 87.8% was achieved after 60 min, at pH 8, and Cd²⁺ initial concentration of 20 mg /L. Thermodynamic parameter suggests that the system is spontaneous and endothermic. Therefore, MSCB exhibits great potential for application in the remediation of wastewater containing Cd²⁺ as a low-cost and eco-friendly adsorbent.

Keywords Adsorption · Modeling · Cadmium · Biochar · Wastewater

1 Introduction

Heavy metals have found extensive applications in many industries to keep up with current technologies because of their structural diversity [1]. Heavy metal pollution is a significant environmental concern because heavy metals are highly toxic, bioconcentrated, and non-biodegradable [2]. These heavy metals accumulate in organisms after ingesting the environment due to their non-degradable abilities, which can lead to numerous cancers and other disorders [3–5]. On the other hand, water contamination and lack of fresh water are the current main global environmental challenges brought on by human activity [6]. In both inorganic and organic aquatic environments, cadmium (Cd²⁺) exists in various chemical and physical forms, including particle, colloidal, and dissolved forms [7]. It is an unneeded element in the human body and typically appears as a mineral alongside other elements, such as oxygen and sulfur [8, 9]. However, Cd²⁺ is the most frequently hazardous heavy metal

✉ Yanting Wang
wyt@mail.hzau.edu.cn

¹ Biomass & Bioenergy Research Centre, College of Plant Science & Technology, Huazhong Agricultural University, Wuhan 430070, China
² Key Laboratory of Fermentation Engineering (Ministry of Education), Hubei Key Laboratory of Industrial Microbiology, Biomass & Bioenergy Research Centre, Hubei University of Technology, Wuhan 430068, China
³ Agricultural and Biosystems Engineering Department, Faculty of Agriculture, Damietta University, Damietta 34517, Egypt
⁴ Radioisotope Department, Nuclear Research Center, Egyptian Atomic Energy Authority (EAEA), Cairo, Egypt

abundantly found in the environment, posing a considerable threat to human health [10, 11]. Due to its high toxicity, it is classified by the European Union as a chemical with a high risk of cancer [12]. It causes severe and irreversible harm to the human body, such as osteoporosis, renal failure, metabolic problems, neurological damage, liver cirrhosis, kidney failure, bone damage, emphysema, anemia, and cancer [13–17]. As a result, the quest for green, cost-effective remediation technologies that can remove it efficiently and affordably has become an essential requirement to protect the natural environment and improve water quality. A wide range of technologies is now being utilized to eliminate heavy metals from water, such as adsorption, membrane separation, capacitive deionization, precipitation, and biological methods [18–23]. However, most of these techniques have significant drawbacks that prevent widespread deployment, such as high costs, poor efficiency, a laborious implementation procedure, and the creation of secondary pollutants [24]. Adsorption is an eco-friendly, highly effective, easy-to-use, cheap, and simple method for eliminating heavy metals from water. It also has a considerable adsorption capacity [25–28]. Although a range of natural and artificial materials have been extensively used as adsorbents, the development of affordable, highly effective, and sustainable adsorbents continues to be the primary concern for guaranteeing the safety of the world's water environment [29–31].

Currently, biochar and agricultural waste serve as cost-effective and energy-efficient adsorbents, and they have been employed successfully to treat polluted wastewater [32]. Biochar, a solid residue produced from the thermal decomposition of biomass, has significant promise for addressing environmental issues. This is owing to its wide range of source materials, abundant functional groups, highly porous structure, vast surface area, and high capacity for ion exchange [33–35]. However, applying raw biochar, generated directly from biomass pyrolysis, is hampered because its surface area, functional groups, and ion exchangeability are generally limited. Several approaches are used to improve the raw biochar's ability to adsorb heavy metals to overcome this issue [36, 37]. Engineered biochar (EBC) is biochar that has been altered using pre- or post-treatment procedures, such as chemical, biological, or physical processes to enhance its capacity to remove or immobilize environmental contaminants [38–40]. One of the best methods for functionalizing biochar is chemical modification, which includes acid/base treatment [41], chemical oxidation [42], and impregnation with mineral oxides [43]. Studies have shown that aluminum (Al) hydroxide/oxide on the surface of adsorbents can enhance the selectivity and efficacy of different pollutants removal in aqueous solutions [44–52]. Despite the exceptional contaminant removal capabilities of metal oxide/hydroxide-loaded EBCs, there has been limited systematic investigation into the influence of feedstock type,

metal cation type, and loading on the Cd^{2+} adsorption efficacy of EBCs [53]. Agricultural waste, animal manure, and municipal waste are among the common raw materials currently being used in biochar production, and they are based on source universality and cost-effectiveness [54].

In several countries, sugarcane (*Saccharum officinarum*) is an extensively grown tropical plant species that makes up a significant fraction of the sugar industries in the world [55]. Among many types of agricultural waste, sugarcane bagasse (SCB), in particular, offers the benefits of being widely available, inexpensive, and biodegradable. It contains around 42% cellulose, 25% hemicellulose, and 20% lignin [56]. Thus, bagasse can be utilized as a raw material instead of typical fossil fuels in producing carbon products, reducing the use of nonrenewable resources. Additionally, by realizing the transformation of waste into health, a significant amount of SCB waste can be used effectively to reduce environmental contamination brought on by inappropriate agricultural waste disposal [57]. Recent evaluations have advocated for the utilization of sugarcane bagasse, both in its raw and processed states, for the elimination of diverse aqueous contaminants [38, 58–62]. Nonetheless, sugarcane bagasse biochar has been insufficiently investigated, and according to the authors' study, it represents a novel material for cadmium adsorption. This adsorbent is cost-effective and practical due to its affordability and availability as agricultural waste. It is regarded as a sustainable and efficient alternative technology. It possesses less operational and production expenses alongside elevated therapy efficacy.

Despite the existing research on biochar as an adsorbent for heavy metal removal, very few comprehensive studies focusing on the optimization of bagasse-derived biochar specifically for efficient Cd^{2+} adsorption, emphasizing the need to fill this research gap and provide insights into the practical implementation and scalability of this eco-friendly solution. RSM is viewed as a powerful mathematical and statistical technique for designing experiments, constructing models by analyzing the effect of numerous operating factors by modifying them simultaneously [63]. The major purpose of RSM is to acquire the optimum operating conditions in a short time with a restricted number of experiments [64–67]. Magnetically modified iron oxide immobilized biochar adsorbent using *Juglans regia* shells and investigate its adsorption capacity for Cu^{2+} and Ni^{2+} removal from synthetic wastewater contaminated with metals by applying Box-Behnken design [68]. Response surface methodology (RSM) has been effectively employed in previous studies to optimize adsorption processes, such as the removal of Cu^{2+} ions using pottery sludge, where the Box-Behnken design was utilized to analyze equilibrium, kinetic, and thermodynamic data [69].

This study aims to assess the efficacy of aluminum hydroxide ($\text{Al}(\text{OH})_3$)-modified biochar, sourced from

sugarcane bagasse, in the effective extraction of cadmium ions (Cd^{2+}) from aqueous solutions by using response surface methodology (RSM), which relies on the Box-Behnken Design (BBD) to discover the ideal conditions for maximum cadmium removal. An investigation was conducted to examine the impact of pH, initial concentration of Cd^{2+} , and duration on the efficacy of Cd^{2+} adsorption by modified biochar. The study also examined the kinetics, thermodynamics, and adsorption isotherms. This research contributes to the field of environmental science by providing a viable solution for cadmium removal, promoting sustainability, and enhancing the value of agricultural waste.

2 Materials and methods

2.1 Feedstock and chemicals

Sugarcane bagasse (SCB) was obtained from a local market located in Sahrajt Al-Kubra village, Daqahliya State, Egypt, at coordinates $30^{\circ}38'21.5''\text{N}$ $31^{\circ}16'56.1''\text{E}$. Before oven drying, the bagasse was immersed and cleansed in distilled water. The drying process lasted for 24 h at a temperature of 80°C . Subsequently, the bagasse was crushed into particles with sizes ranging from 0.1 to 0.2 mm. The SCB was compressed and stored in airtight polythene bags for future use. All substances used in this experiment were of analytical grade. A solution of cadmium was formed by dissolving it in distilled water, resulting in a concentration of 1000 mg/L. The addition of distilled water led to different amounts of Cd^{2+} . To change the pH, acid and base solutions with 0.1 M HCl and NaOH were prepared, respectively.

2.2 MSCB preparation

A specific quantity of powdered bagasse was submerged overnight in 200 mL of a 5% (w/v) $\text{Al}(\text{OH})_3$ solution at room temperature. The mixture was oven-dried at 90°C and then placed in an oxygen-free muffle furnace at 350°C for 60 min [70]. The reactor's temperature was systematically raised at a constant rate of 10°C per minute. After the pyrolysis process was completed, the reactor was allowed to cool down to the temperature of the surrounding environment, and the modified sugarcane bagasse biochar (MSCB) was collected and used in further analysis/experiments (Fig. S1).

2.3 Adsorbent characterization

The surface morphology of MSCB was examined using an energy-dispersive X-ray spectrometer (EDX) and scanning electron microscopy (SEM) both before and after adsorption. The material's principal functional groups were identified using (FTIR) spectrophotometer (Thermo-Scientific, Nicolet

iS50, USA) both before and after the transformation. The Rigaku MiniFlex 600 diffractometer was utilized in X-ray diffraction (XRD) investigations, where Cu Ka radiation was employed. BET test was engaged to precisely evaluate the surface area, pore volume, and pore size distribution. Furthermore, a nitrogen adsorption/desorption experiment was conducted at a temperature of 77 K utilizing a Quantachrome Nova Touch LX2 analyzer model.

2.4 pH_{PZC} of prepared MSCB

The salt addition method was employed to ascertain point of zero charge (pH_{PZC}) of MSCB [71]. More precisely, 40 mL of sodium nitrate (0.1 M) was gathered and distributed evenly among eight separate Erlenmeyer flasks. The pH was modified within the range of 3 to 10. Subsequently, 0.02 g of MSCB was introduced into each flask and well-mixed overnight at 150 rpm under a temperature of 30°C . Once equilibrium was reached, the contents were subjected to filtration, and the pH of the resulting filtrates was measured. The MSCB pH_{PZC} value, which represents the pH at which the adsorbent's overall surface charge reaches neutrality, was established by plotting the initial pH against the subsequent pH reduction.

2.5 Adsorption experiment

The produced adsorbent was utilized for Cd^{2+} adsorption. The studies were carried out in batch mode, where the adsorbent (MSCB) was combined with cadmium solution in an Erlenmeyer conical flask. The following equations were used to compute the removal efficiency ($R\%$) and adsorption capacity (q_e , mg/g):

$$R(\%) = \frac{c_0 - c_e}{c_0} \quad (1)$$

$$q_e = \frac{C_0 - C_e}{w} \times v \quad (2)$$

The variables in the equations are as follows: W represents the mass of adsorbent utilized in grams (g); V represents the volume of the reaction solution in liters (L); and C_0 and C_e represent the initial and final concentrations of cadmium in milligrams per liter (mg/L), respectively. Using the RSM (Sect. 2.6), the adsorption parameters pH, cadmium concentration, and time were optimized. Cd^{2+} adsorption kinetics, isotherms, and thermodynamic investigations were carried out at optimized conditions. The starting concentration was varied from 10 to 80 ppm to record the adsorption isotherms. Similarly, the contact period was varied from 15 to 480 min for the kinetics investigation. The adsorption thermodynamic studies were conducted at three distinct

temperatures: 298, 313, and 328 K. The adsorption experiment was carried out with optimized adsorption parameters. Before the final concentration analysis, all samples underwent filtration using a 0.45- μm filter. A nuclear adsorption spectrophotometer (Perkin-Elmer 2380) was used to measure the Cd^{2+} percentage in the filtrates.

2.6 Box-behnken experimental design

Cd^{2+} removal efficiency was optimized using a factorial experimental approach. The performance of the Box-Behnken design (BBD) is optimal for a three-factor response surface methodology (RSM) problem. The parameters in this investigation were pH, initial Cd^{2+} concentration, and adsorption time. Three levels — high (1), middle (0), and low (−1) — were assigned to the components, which were referred to as *A* (pH), *B* (Cd^{2+} concentration), and *C* (time). Modeling and analysis with (RSM), a set of statistical and mathematical techniques for creating experiments with multivariate components, was used to modify the response values. BBD model was employed in this work to explore the effects of pH (*A*, 4–8), Cd^{2+} concentration (*B*, 20–80 mg/L),

and time (*C*, 30–90 min) on the removal of Cd^{2+} by utilizing a constant amount of 0.1 g of MSCB (Table 1). The response value was the Cd^{2+} adsorption efficiency (*R*%). In total, 17 runs for a three-parameter experimental design were carried out at the individual and combined impacts of various conditions on adsorption efficiency. ANOVA statistical analysis was performed with Design Expert 13 to evaluate the model's relevance and significance. The model's statistical significance was determined using the *F*-value and *P*-value 0.05 at the 95% confidence range.

3 Results and discussion

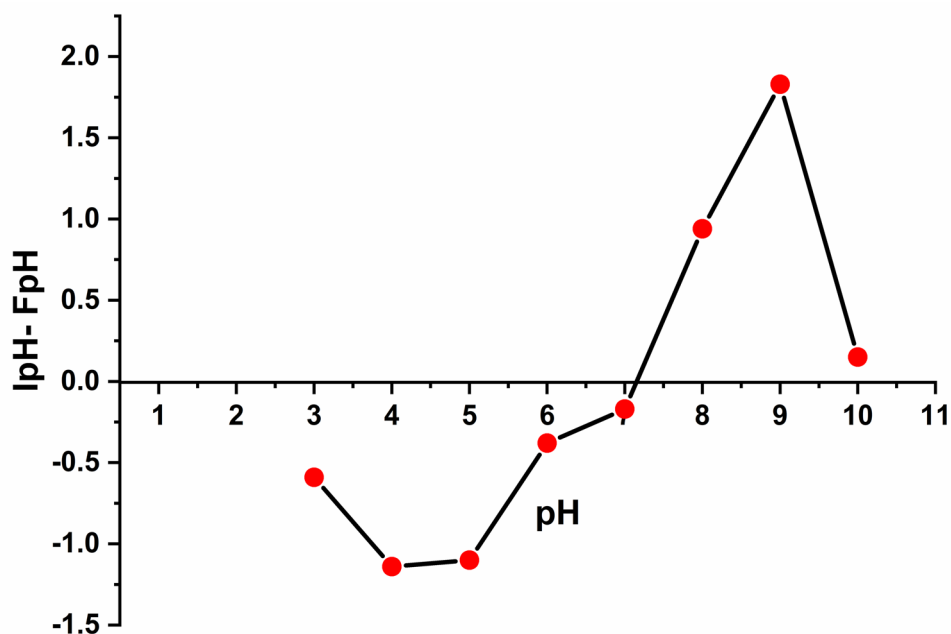
3.1 Point of zero charge

The pH_{PZC} is the pH at which the functional group does not participate in adsorption. The preferability of the adsorbed cations is greater than pH values higher than the pH_{PZC} [72]. Based on the calculation, the adsorbent's (pH_{PZC}) was determined to be 7.25, suggesting that it had certain alkaline characteristics (Fig. 1). When the pH of the solution containing the substance to be adsorbed dropped below the point of zero charge (pH_{PZC}), the surface charge of the adsorbent became positively charged. Nevertheless, when the pH exceeded the point of zero charge (pH_{PZC}), the surface charge of the adsorbent turned negative [73]. Consequently, the surface charge of the MSCB was positively charged in acidic conditions, leading to a decrease in the absorption of Cd^{2+} . A pH level above 7.25 in the solution containing the substance being adsorbed resulted in a negative charge on the surface,

Table 1 Experimental level of independent variables for Cd^{2+} adsorption using Box-Behnken design

Independent variables	Symbol	Coded levels		
		−1	0	+1
pH	X_1	4	6	8
Cd^{2+} concentration (mg/L)	X_2	20	50	80
Time (min)	X_3	30	60	90

Fig. 1 Point of zero charge of the MSCB



leading to an increase in adsorption of Cd^{2+} . Moreover, an increased pH level can modify the chemical makeup of the functional groups, hence impacting the adsorption process [74–78].

3.2 Characterization of sugarcane bagasse-derived biochar

3.2.1 SEM analysis

The surface morphology of MSCB was examined before and after cadmium adsorption (Fig. 2). SEM scans indicated that the surface of MSCB, initially coarse, became fairly smooth following the adsorption of Cd^{2+} . This occurs because when MSCB undergoes pyrolysis at a designated temperature, it transforms into biochar characterized by a porous structure. This porous biochar possesses an increased surface area, hence augmenting its capacity to absorb pollutants [79]. The SEM scans indicated that MSCB exhibited numerous holes and pores on its surface, potentially increasing active sites for adsorption. The surface morphology of MSCB was irregular, coarse, and heterogeneous, featuring prominent voids that were extensively dispersed across the MSCB surface as a result of the modification of a polymeric matrix with aluminum hydroxide. A substantial amount of debris is observed in the MSCB SEM image, which formed pores in the biochar that facilitate the ingress of heavy metal ions. Numerous crystal particles are detected to have formed on the biochar surface in the SEM image of MSCB after adsorption, as depicted in Fig. 2b, and EDX analysis indicates that these particles contain Cd^{2+} elements.

3.2.2 EDX analysis

The results demonstrated that Cd^{2+} in solution may be adsorbed into MSCB by surface chemical adsorption. The EDX spectra and element analysis of MSCB and MSCB + Cd^{2+} are given in Fig. 3. As can be observed from Fig. 3, MSCB contains C, O, Al, K, Ca, and Mo elements, while the spectra of MSCB + Cd^{2+} demonstrate the existence of Cd^{2+} and that means the success of adsorption process. Following adsorption, the K element content decreased from 0.69% in MSCB to 0% in MSCB + Cd^{2+} . In comparison, the Mo element content decreased from 1.66 to 0%, indicating that K and Mo had an ion exchange reaction with Cd^{2+} and transferred Cd^{2+} elements from water to biochar. Furthermore, the EDX analysis showed a general minor elevation in the elemental contents of C and O of the MSCB after the adsorption of Cd^{2+} . This observation reconfirmed the loading of cadmium molecules on the surface of the MSCB by adsorption mechanism.

3.2.3 BET analysis

The BET surface area of biomass-derived biochar is affected by various factors, including the composition of the parent biomass, the heating rate during the pyrolysis process, and the pyrolysis temperature itself. The present study detected that the MSCB prepared at a pyrolysis temperature of 350 °C exhibited a surface area of 15.17 m^2/g . The BET and N_2 adsorption–desorption isotherms of MSCB are shown in Table 2 and Fig. 4. The result reflects a relatively high surface area of MSCB compared to the surface area of SCB (4.70 m^2/g); MSCB and SCB have an average pore size of 7.87 nm and 11.31 nm, respectively, making them mesoporous and appropriate for adsorption materials [80].

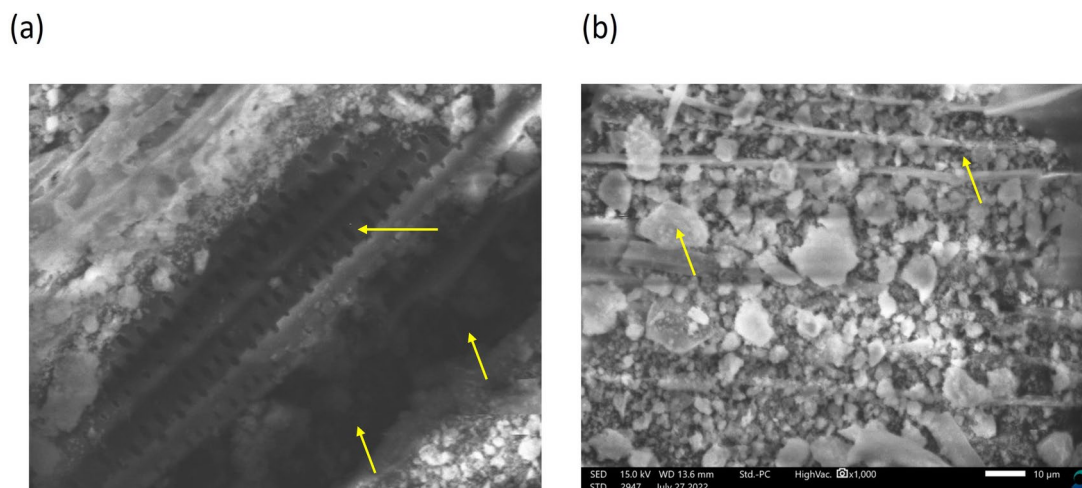


Fig. 2 SEM image of modified sugarcane bagasse biochar (MSCB) before (a) and after (b) adsorption

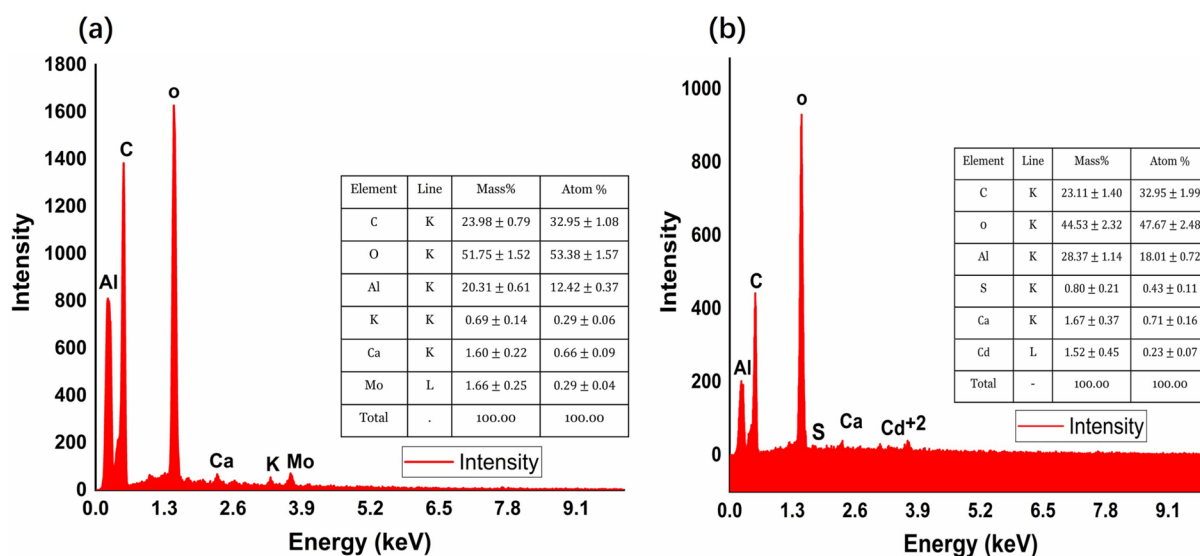


Fig. 3 EDX image of MSCB before (a) and after (b) adsorption

Table 2 BET analysis of SCB and MSCB

Material	BET surface area (m ² /g)	Total pore volume (cm ³ /g)	Average pore size (nm)
SCB	4.70	0.01	11.31
MSCB	15.17	0.06	7.87

3.2.4 XRD analysis

The XRD pattern of MSCB before and after adsorption is presented in Fig. 5 showing numerous sharp and distinguished peaks observed at $2\theta = 26.70^\circ$, 36.59° , 42.86° , 48.02° , 63.22° , and 76.42° . These sharp peaks reflect that the MSCB was more crystalline and less amorphous. The prominent peak between 20 and 30° of MSCB indicates disordered carbon with high carbon content, corresponding with the morphological surface from the SEM picture [80]. The characteristic peaks of XRD after adsorption indicated the presence of C, Al₂O₃, and Cd H₂O₂ (Card

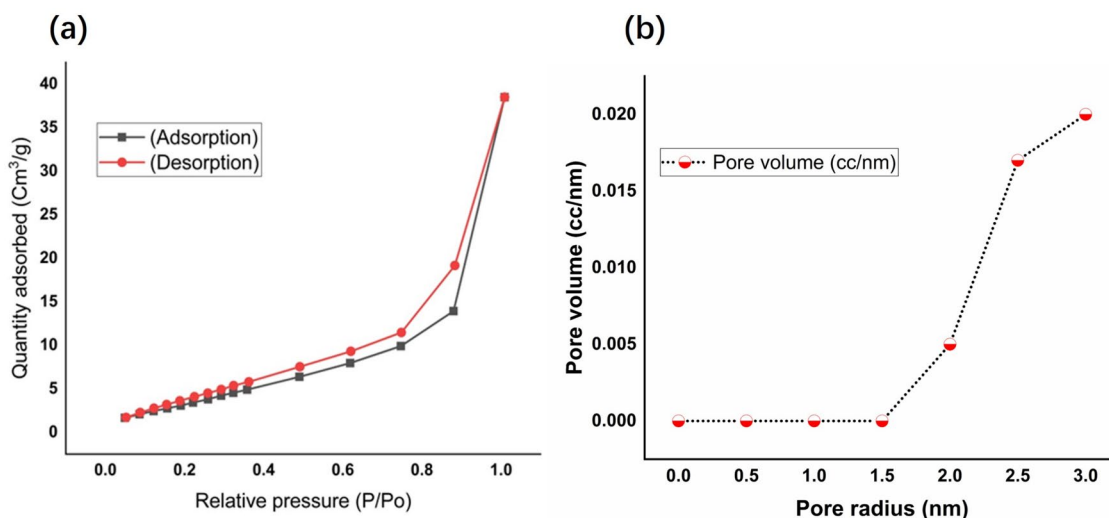


Fig. 4 BET analysis of MSCB for N₂ adsorption–desorption isotherms and pore size distribution

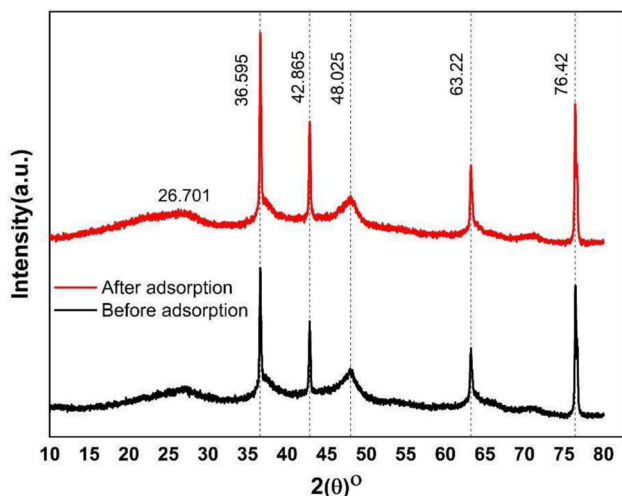


Fig. 5 XRD pattern of MSCB before and after adsorption

Number: 9012590, 1,200,005, and 2,310,422), respectively. The adsorption process occurred primarily on the material's surface without significantly altering its internal crystal structure, as indicated by the similarity in XRD peaks before and after adsorption. This can shed light on the adsorption mechanism and the adsorbent material's stability as the process progresses. Scherrer equation Eq. (3) measured crystalline size as 23.64 nm.

The Scherrer equation is given by:

$$D = \frac{k \cdot \lambda}{\beta \cos(\theta)} \quad (3)$$

where D = crystallite size, K = shape factor (0.9), λ = wavelength of the X-ray radiation (0.15406 nm), β = FWHM of the peak (in radians), and θ Bragg angle (in radians).

3.2.5 FTIR examination

FTIR was conducted to detect distinct functional groups current on the adsorbent before and after modification. As shown in Fig. 6, the MSCB before and after modification shows peaks at 3700 cm^{-1} , which signify the (O–H) stretching vibration of hydroxyl and carboxyl oxygen-containing functional groups. Similarly, $2850\text{--}3000 \text{ cm}^{-1}$ peaks indicated the presence of saturated alkane (C–H). In addition, FTIR peaks detected at 2210 cm^{-1} may be attributed to the stretching vibration of esters, aldehydes, and carboxylic acids C–O groups, while the peaks at 1810 cm^{-1} , 1600 cm^{-1} , $1500\text{--}1410 \text{ cm}^{-1}$, 1310 cm^{-1} , 1270 cm^{-1} , 1150 cm^{-1} , $1110\text{--}1070 \text{ cm}^{-1}$, and $971\text{--}739 \text{ cm}^{-1}$ showed the presence of (C=O), (C=C), (C–O), (CH₂), (–CO), (C–O–C), and aromatic ring of organic compounds (C–H). 638 cm^{-1} would be halogen groups. The peaks of 3000 cm^{-1} and 971 cm^{-1}

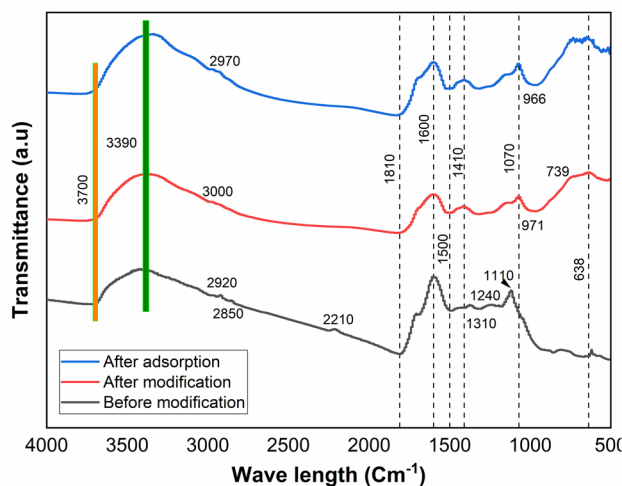


Fig. 6 FT-IR spectra of MSCB before and after modification

before adsorption converted to 2970 cm^{-1} and 966 cm^{-1} . At the same time, 638 cm^{-1} disappeared after adsorption, and this could provide the presence of cadmium after adsorption [74, 81–85].

3.3 Model analysis

3.3.1 Regression model

Response surface methodology (RSM) is a statistical technique that utilizes multivariable nonlinear modeling to create mathematical models that accurately represent the data collected via experimental design. Consequently, the statistical significance of the impacts of the components and their interactions is elucidated more explicitly. Design-Expert 13.0 software is employed in the experimental design for response surface analysis to conduct regression analysis and equation fitting. This software utilizes mathematical models to elucidate the correlation between input elements and response variables, simplifying the process of modeling and optimizing intricate experimental systems. The independent variables used for the experiment were pH (A), Cd^{2+} concentration (B), and time (C). These variables were selected to achieve the highest possible response. The examination was conducted for each element at three different levels. To optimize the tests and evaluate the removal efficiency of Cd^{2+} , the Box-Behnken design (BBD) was utilized. The results acquired from this design are summarized in Table S1. The quadratic regression model for the response variable, denoted as Yq , is represented by Eq. (4).

$$Yq = +37.95 + 22.72A - 16.23B + 1.59C - 7.05AB + 1.67AC + 3.65BC - 1.58A^2 + 4.03B^2 - 0.1814C^2 \quad (4)$$

where A is the pH; B is the Cd^{2+} concentration (mg/L); and C is the time (min).

In the quadratic regression model equation, A , B , and C represent linear terms, AB , AC , and BC represent interaction terms, and A^2 , B^2 , and C^2 represent quadratic terms. In the aforementioned equation, the positive or negative sign preceding a coefficient indicates the nature of the interaction between the variables. A positive sign signifies a cooperative interaction, indicating that the variables have a synergistic effect on each other. Conversely, a negative sign indicates an opposing interaction, suggesting an antagonistic effect between the variables. Analyzing Eq. (4), it can be observed that the variables pH and Cd^{2+} concentration exhibit antagonistic effects on each other, meaning that their combined influence is less than their individual effects. On the other hand, the variables pH and time, as well as Cd^{2+} and time, demonstrate synergistic effects.

3.3.2 ANOVA analysis

The variance of the experimental data is examined using the quadratic regression model, and the results are presented in Table S2. The model's applicability was determined based on a p -value of less than 0.05 and a higher F -value. As shown in Table S2, the p -value is less than 0.0001, and

the F -value is 131.27, representing that the model is highly suitable for this experiment. The correlation coefficient values for model fitting ($R^2=0.9941$) and adjusted R^2 ($R^2_{\text{adj}}=0.9865$) demonstrate a strong agreement between the experimental results and the quadratic regression model. Additionally, the adequacy precision of the model, with a value of 42.9841, is considerably greater than 4, further supporting the model's reliability. Based on the p -values in Table S2, it can be observed that variables A , B , AB , BC , and B^2 are significant ($p < 0.05$), while variables C , AC , A^2 , and C^2 are non-significant ($p > 0.05$). In the regression models, the F -values for variables A , B , and C are 739.52, 377.47, and 3.63, respectively. This indicates that parameter A has the greatest effect on the adsorption performance of MSCB biochar, followed by parameter B , while parameter C has the least significant influence. Regarding the interaction terms, the effects are ranked as follows: $AB > BC > AC$, indicating that AB has the most substantial impact on the adsorption performance of MSCB biochar, followed by BC , and then AC .

3.3.3 Model parameters' effects and interactions

According to the three-dimensional (3D) response surface and respective contour plots (Fig. 7a), the interactive

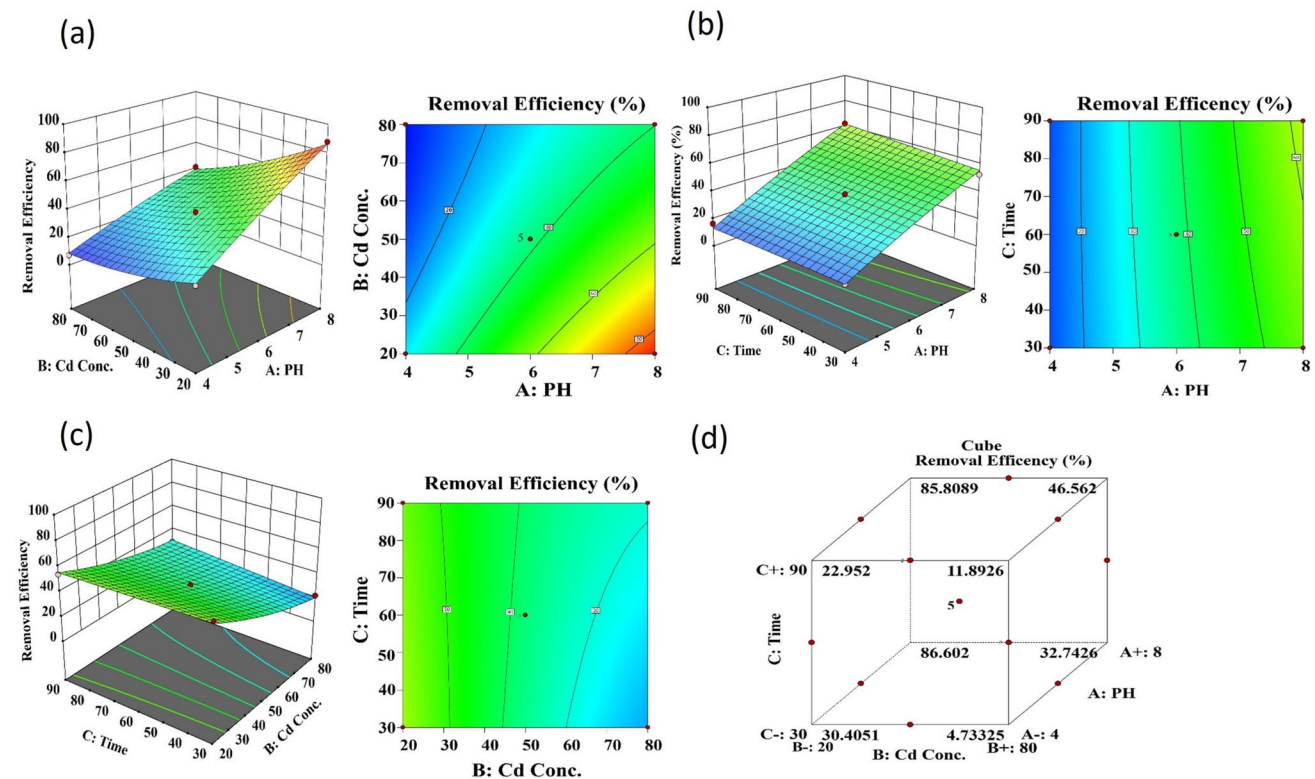


Fig. 7 The combined effect of process variables **a** pH and cadmium concentration, **b** pH and time, **c** cadmium concentration and time on cadmium removal efficiency, and **d** removal percentage of cadmium at each factorial point

effect of pH and initial cadmium concentration on cadmium removal efficiency is highly significant as cadmium adsorption increases from 7.06 to 87.83% when the pH is increased from 4 to 8. This is also consistent with the ANOVA analysis of *AB* ($p=0.0006$; $F=35.58$; Table S2). Furthermore, Fig. 7b shows a link between pH and time, with no substantial influence on cadmium elimination. Cadmium removal effectiveness rises from 13.36 to 87.83% by increasing the response time from 30 to 60 min and then decreasing from 60 to 90 min. This is also in keeping with the ANOVA analysis of *AC* ($p=0.2016$; $F=1.99$; Table S2). However, a significant interaction impact ($p=0.0175$; $F=9.56$) is detected between the initial concentration of cadmium and reaction time, as shown in Table S2 and Fig. 7c. As the pH of Cd^{2+} climbs from 4 to 8, the percentage removal likewise increases. At a low pH value, the absorption % is low, which may be due to protonation on the surface of the adsorbent, resulting in electrostatic repulsion between the adsorbent and Cd^{2+} ions in the same line with a point of zero charge value. Consistent findings have been informed in several studies, indicating that the adsorption capacity of adsorbents is generally lower at acidic pH levels, while it tends to increase as the pH becomes higher [86–91].

When the pH falls below 7.25, the MSCB surface becomes positively charged. The presence of a positive charge causes electrostatic repulsion of positively charged Cd^{2+} ions from the surface. This repulsion interferes with ion adsorption. Moreover, an increased amount of H^+ ions in the solution vies with Cd^{2+} ions for the existing adsorption locations, leading to a decrease in the adsorption of Cd^{2+} . Conversely, the rise in adsorption observed at elevated pH levels can be linked to the idea that metal cations with positive charges encounter less resistance from oxide surfaces as the pH level rises.

As the solution's pH rises, the quantity of positively charged locations on the adsorbent's surface decreases, whereas the quantity of negatively charged locations rises. This change towards a negatively charged surface encourages capturing cationic Cd^{2+} ions through electrostatic attraction. Additionally, with the increase in the concentration of the Cd^{2+} solution, the quantity of Cd^{2+} captured (q_e) also rises. Nonetheless, as the solution concentration rises, the removal rate ($R\%$) diminishes. This suggests that an elevated concentration of Cd^{2+} in the solution results in a greater adsorption capacity by the adsorbent, yet the removal effectiveness diminishes. In instances where the initial solution concentration was minimal, the surface area and the number of available adsorption sites were comparably extensive. Moreover, the Cd^{2+} ions were readily captured and eliminated from the solution. As the initial solution concentration rises, the available adsorption sites become limited, decreasing the percentage of Cd^{2+} ion removal. The

higher q_e observed at elevated initial concentrations can be attributed to a stronger driving force [92].

During the first step of the adsorption process, the mesopores are nearly saturated with Cd^{2+} ions. The Cd^{2+} ions must, therefore, go farther and deeper into the micropores, facing significantly higher resistance, resulting in lower driving force and adsorption rate. Furthermore, when the adsorption process progresses and the desorption rate increases, the adsorption–desorption equilibrium is also influenced [88, 93–97]. These findings might be important for increasing and optimizing the Cd^{2+} removal process in real wastewater treatment operations, perhaps leading to significant increases in treatment efficacy. The best conditions for the maximal adsorption of Cd^{2+} ions from aqueous solution utilizing MSCB as an adsorbent is pH 8, 20 mg/L initial concentration of cadmium ions and 60 min contact time. At these ideal circumstances, the highest adsorption was recorded at 87.83%, and the removal percentage of cadmium at each factorial point is shown in Fig. 7d.

3.3.4 Model data adequacy check

In the BBD experimental design, a variance analysis was conducted on the gathered experimental data. The actual data points were obtained through experimental measurements, while the expected response, represented by the removal efficiency percentage was generated using the RSM model. Figure 8 illustrates that all the data points lie along the diagonal line connecting the predicted and actual values. It is worth noting that previous research has shown that data

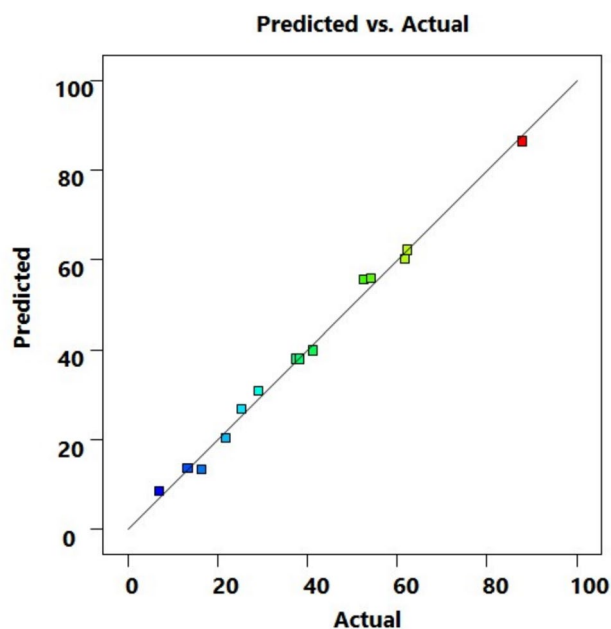


Fig. 8 The plot of predicted vs. actual Cd^{2+} removing efficiency

points aligning with this line indicate the adequacy of the model. As depicted in Fig 8, the actual data points closely match the projected values, further validating the accuracy and suitability of the model.

3.3.5 Optimization using the desirability functions

Statistical optimization of the adsorption process was done to get the desired goal such as maximize, minimize, within the range, target, and none for the factors and responses. Numerical optimization sought to determine the optimal value for each input factor and response. The inputs in this study are pH, Cd²⁺ concentration, and contact time with the response being removal efficiency. The numerical optimization of the software demonstrated the optimal removal of Cd²⁺ was obtained at pH 8, 20 mg/L initial Cd²⁺ concentration, and 60-min contact time, as a result. As shown in Fig. S6, the maximal removal of Cd²⁺ is found to be 86.39% with a desirability of 0.98. The validity of this prediction was checked by duplicate confirmatory experiments under the optimized parameters. Overall, the results obtained from experimental data were in a good agreement with data obtained from numerical optimization using desirability functions. This indicated that the RSM-BBD model with desirability functions can be effectively used for optimizing the experimental conditions of Cd²⁺ adsorption by MSCB.

3.4 Adsorption isotherm

The adsorption isotherm equilibrium elucidates the correlation between the surface area of an adsorbent and the concentration of the adsorbate. The calculation of the experimental adsorption data involved using different isotherm models. This study employed the Langmuir, Freundlich, Temkin, and Dubinin-Radushkevich adsorption isotherms. It is assessed whether a certain adsorption isotherm can illuminate the gathered data by the correlation coefficient (R^2) of the summed profile. MSCB was applied to remove Cd²⁺ from a 50 mL solution having various initial Cd²⁺ concentrations (10–80 mg/L), while the other parameters remained constant.

3.4.1 Langmuir isotherm

The Langmuir model illustrates the process by which a monolayer of adsorbate molecules is formed on a surface that is uniformly covered with adsorbent material. According to this hypothesis, no further adsorption will occur once a uniform monolayer is formed. The Langmuir isotherm occurs when a monolayer is adsorbed onto a surface with a specific number of identical spots. There is no communication or influence between the molecules being adsorbed on the surface. Additionally, it is assumed that the energy levels

of each location on the surface where adsorption occurs are the same [98]. The Langmuir plots, depicted in Fig. S2a, are generated by plotting $1/q_e$ against the reciprocal of the equilibrium concentration ($1/C_e$). Equations (5) and (6) are utilized to obtain the constants q_{\max} and K_L from the intercept and slope of the Langmuir plot. An analysis of the Langmuir plot and associated constants indicated that the adsorbent's highest possible adsorption capacity (q_{\max}) was 16.87 mg/g.

$$q_e = \frac{q_{\max} \times k_L c_e}{1 + k_L c_e} \quad (5)$$

To determine the adsorption parameters, the Langmuir's isotherm was converted into its linear form, as illustrated in the following equation:

$$\frac{1}{q_e} = \frac{1}{k_L q_{\max}} \times \frac{1}{c_e} + \frac{1}{q_{\max}} \quad (6)$$

The variable q_{\max} indicates the maximum adsorption capacity of the test beads in milligrams per gram (mg/g), while K_L is the Langmuir isotherm constant, which quantifies the binding affinity between Cd²⁺ and the test beads in liters per milligram (L/mg).

The separation factor (R_L) was derived as follows:

$$R_L = \frac{1}{1 + c_0 \times k_L} \quad (7)$$

Adsorption can be classified into four categories based on the dimensionless Langmuir constant: favorable ($0 < R_L < 1$), unfavorable ($R_L > 1$), linear ($R_L = 1$), or irreversible ($R_L = 0$) [99].

3.4.2 Freundlich isotherm

Based on the Freundlich isotherm model, the adsorption of Cd²⁺ occurs on a surface that is not uniform, and it happens through the formation of several layers. As the concentration of Cd²⁺ grows, the amount of adsorbate that is adsorbed also increases without limit [98]. According to this notion, the adsorption process encompasses many adsorption energies. The Freundlich isotherm Eq. (8) establishes a relationship between the amount of adsorbate adsorbed per unit mass of adsorbent (q_e) and the equilibrium concentration of Cd²⁺ (C_e). The adsorption plot of Cd²⁺ onto MSCB is depicted in Fig. S3b. By analyzing the Freundlich isotherm plot, the values of the Freundlich constants were determined. The K_f value for the adsorption of Cd²⁺ molecules by MSCB, as reported in this work, is 5.91. The corresponding $1/n$ values are 0.29, with n being 3.389. The magnitude of the exponent $1/n$ serves as an indicator of the favorability of adsorption. In this case, the calculated values show that the adsorption of Cd²⁺ onto MSCB is favorable.

$$q_e = k_f C_e^{1/n} \tag{8}$$

The term $1/n$ denotes the degree of adsorption, while K_f , known as Freundlich’s constant, is utilized to calculate the adsorption capacity. The value of $1/n$ determines the favorability of the adsorption process, with a range of $0.1 < 1/n < 0.5$ indicating favorability and $1/n > 2$ indicating unfavorability [78, 80, 100].

3.4.3 Temkin isotherm

The Temkin isotherm model describes the relationship between the reduction in adsorption energy and the surface coverage resulting from interactions between the adsorbent and adsorbate. According to this model, the drop in adsorption energy is directly related to the surface coverage rather than having a logarithmic relationship. The Temkin isotherm assumes a uniform distribution of binding energies. To derive the constants of the Temkin isotherm model, the quantity adsorbed (q_e) is plotted against the natural logarithm of the equilibrium concentration ($\ln C_e$). By analyzing the resulting graph and calculating the slope and intercept, the constants of the Temkin isotherm equation can be determined in Fig. S4c. The linear version of the Temkin isotherm is signified by Eq. (9):

$$q_e = B \ln A + B \ln C_e \tag{9}$$

The formula for B is $B = RT/bT$, where T is the absolute temperature in Kelvin, and R is the universal gas constant (8.314 J/mol K). The quantity of metal ions adsorbed onto the adsorbent at equilibrium is denoted by q_e (mg/g). The equilibrium binding energy and heat of sorption are denoted by the Temkin parameters A and B , respectively.

3.4.4 D-R isotherm

The Dubinin-Radushkevich (D-R) isotherm model was employed to ascertain the nature of adsorption, whether it was chemical or physical [101]. The Dubinin-Radushkevich plot is shown in Fig. S4d, and its Eqs. (10), (11), and (12) are shown as follows:

$$\ln q_e = \ln q_m - K_\epsilon^2 \tag{10}$$

The equation is defined as follows: K represents the activity coefficient (mol^2/KJ^2); ϵ represents the Polanyi potential (KJ mol^{-1}), and q_e represents the equilibrium adsorbent-phase concentration of adsorbate (mg/g).

$$\epsilon = RT \ln 1 + 1/c_e \tag{11}$$

$$E = \frac{1}{\sqrt{2k}} \tag{12}$$

where T represents the temperature in Kelvin (K); C_e represents the equilibrium concentration of the adsorbate in the aqueous phase (mg/L); and R represents the universal gas constant (J/mol K).

The comparison of four adsorption isotherm models (Langmuir, Freundlich, Temkin, and Dubinin-Radushkevich) is performed, and the evaluation is based on the correlation coefficient (R^2) and related parameters, as presented in Table 3. The obtained findings revealed that the regression coefficients (R^2) for the Langmuir, Freundlich, Temkin, and Dubinin-Radushkevich models were 0.99, 0.90, 0.97, and 0.93, respectively. Based on the comparison of the correlation coefficients (R^2), the Langmuir adsorption isotherm model ($R^2 = 0.99$) demonstrated the best fit for Cd^{2+} adsorption onto MSCB. This suggests that the Langmuir model gives a more realistic depiction of the connection between the numbers of Cd^{2+} molecules adsorbed by the MSCB adsorbent. The Langmuir model is in a reasonable covenant with the observed experimental results due to its assumption of a homogeneous of active sites on the surface of the MSCB adsorbent so the Langmuir model was shown to be the most accurate and relevant model in this study for characterizing the adsorption behavior of Cd^{2+} on MSCB, suggesting the chemisorption mechanism [74].

3.5 Adsorption kinetic models

The experimental results were calculated using several kinetic parameters to better understand the mechanism that regulates the adsorption process. Kinetic models are used not only to measure the effective diffusion of adsorbate molecules in the pore structure but also to calculate and

Table 3 Isotherm parameters for the adsorption of Cd^{2+} by MSCB

Isotherm model	Parameters	Value
Langmuir	q_{\max} (mg/g)	16.87
	K_L (L/mg)	0.42
	R_L	0.03
	R^2	0.99
Freundlich	K_F	5.91
	$1/n$	0.29
	R^2	0.90
Temkin	KT (L/mg)	7.46
	BT (J/mol)	2.91
	R^2	0.97
D-R	K	2.51×10^{-9}
	E	1.41×10^4
	R^2	0.93

quantify the adsorbate's absorption by the adsorbent over time at a fixed concentration [102]. To ascertain the rate and mechanism of metal absorption, the data was analyzed using pseudo-first- and pseudo-second-order models [103].

3.5.1 Pseudo-first order

The adsorption capacity of the adsorbent is employed in the pseudo-first-order rate model following Eq. (13):

$$\ln(q_e - q_t) = \ln q_e - k_1 t \quad (13)$$

where K_1 (min^{-1}) is the equilibrium rate constant, and q_t is the adsorption capacity (mg/g) at time t .

According to the information provided, Fig. S3a depicts experimental kinetic plots of Cd^{2+} adsorption onto MSCB using the pseudo-first-order model. Plots of the natural logarithm of the difference between the adsorption capacity at a given time (q_t) and the equilibrium adsorption capacity (q_e) vs. time produce a straight line. The slope and intercept of these plots were used to derive the rate constant (K_1) and equilibrium adsorption capacity (q_e). However, considerable variations are discovered when comparing the projected equilibrium adsorption capacity (q_{cal}) with the actual equilibrium adsorption capacity (q_{exp}), as illustrated in Table 4. The adsorption data reveal low correlation coefficients, and the maximal adsorption capacity differs from the actual value. These observations suggest that the Cd^{2+} adsorption onto MSCB does not conform to the assumptions and hypothesis of the pseudo-first-order kinetics model. It appears that the pseudo-first-order kinetics model is not fit for accurately describing the adsorption behavior of Cd^{2+} onto MSCB in this case. Alternative kinetic models or further investigations may be required to better understand the adsorption kinetics of Cd^{2+} onto the MSCB adsorbent.

3.5.2 Pseudo-second order

The following equation represents pseudo-second order:

Table 4 Pseudo^{1st} order and pseudo^{2nd} order kinetic parameters for Cd^{2+} adsorption by MSCB

Adsorbent	Kinetic models	Parameters	Cd^{2+}
MSCB	Pseudo ^{1st} order	q_e (cal) mg/g	0.52
		K_1 (1/min)	-2.35×10^{-5}
		R^2	0.76
	Pseudo ^{2nd} order	q_e (cal) mg/g	8.82
		q_e (exp) mg/g	8.75
		K_2 (g/mg·min)	0.06
	R^2	0.99	

$$\frac{t}{q_e} = \frac{1}{k_2 q_e^2} + \frac{1}{q_e} \quad (14)$$

The equilibrium rate constant is K_2 . The linear coefficient of regression (R^2) values is used to estimate the appropriate isotherm and kinetic model for the adsorption process. The plots of t/qt vs. t in Fig. S3b provide a straight line that best fits the experimental results. The analysis of the plots, supported by the slope and intercept values presented in Table 4, indicates a close agreement between equilibrium adsorption capacities (q_e) considered using the pseudo-second-order model and the corresponding experimental value (q_{exp}).

The correlation coefficients (R^2) attained from comparing the two kinetic models, namely the pseudo-first order and pseudo-second order, indicate that the pseudo-second-order kinetics model ($R^2=0.99$) provides a significantly better fit to the experimental data compared to the pseudo-first-order kinetics model ($R^2=0.76$). This is evident from Fig. S3b, which displays the plot generated by the pseudo-second-order model and demonstrates a high correlation coefficient ($R^2=0.99$). These findings suggest that the kinetics of Cd^{2+} adsorption onto MSCB closely adhere to the pseudo-second-order kinetic model. This implies that the adsorption process is likely governed by chemisorption, involving electron exchange between the adsorbate (Cd^{2+}) and the adsorbent (MSCB). The high correlation coefficient ($R^2=0.99$) achieved from the pseudo-second-order model further supports this hypothesis. Therefore, based on the supplied results, it can be assumed that the rate of Cd^{2+} adsorption onto MSCB is largely affected by a chemisorption process, including electron exchange between the adsorbate and adsorbent.

3.6 Adsorption thermodynamics

The study focused on examining the energy transformations that occur during the process of adsorption, using principles from the field of thermodynamics. The thermodynamic parameters entropy (S), Gibbs free energy (G), and enthalpy (H) were computed using Eqs. (15), (16), and (17), correspondingly. The slope and intercept of the $\ln K_L$ vs. $1/T$ plot, as well as the accompanying results, are reported in Fig. S4 and Table 5.

$$\Delta G^0 = -RT \ln KT \quad (15)$$

$$k_L = \frac{q_e}{c_e} \quad (16)$$

$$\ln k_L = \frac{\Delta S^0}{R} - \frac{\Delta H^0}{RT} \quad (17)$$

Table 5 Thermodynamic parameters for the adsorption of Cd²⁺ onto MSCB

Adsorbent	Temp (K)	K_L	ΔG^0 (kJ/mol)	ΔH^0 (kJ/mol)	ΔS^0 (J/mol·K)	R^2
MSCB	298	4.18	-3.54	126.42	434.49	0.97
	313	26.16	-8.49			
	328	454.04	-16.68			

where K_L (L/g) is the equilibrium constant; C_e (mg/L) is the equilibrium concentration of adsorbate; q_e (mg/g) is the amount of adsorbate adsorbed at equilibrium; ΔG^0 (KJ/mol) is the Gibbs free energy change; ΔH^0 (KJ/mol) is the enthalpy change; and R (8.314 J/mol·k) is universal gas constant; while the absolute temperature in Kelvin is T (K).

Thermodynamic investigations were conducted to examine the adsorption of Cd²⁺ on MSCB at three different temperatures: 298 K, 313 K, and 328 K. The initial cadmium concentration used in the experiments was 50 mg/L. The negative values of ΔG^0 , ranging from -3.54 to -16.68 kJ/mol, specify that the adsorption process of Cd²⁺ on MSCB is thermodynamically feasible and spontaneous. This suggests that the affinity of MSCB for Cd²⁺ is strong, and the adsorption occurs naturally without needing external energy input. The positive value of ΔS^0 indicates an increase in unpredictability or randomness during the adsorption process. This is likely attributed to the adsorption of water molecules at the solid-solution interface, which contributes to the overall entropy change. The presence of water molecules enhances the disorderliness of the system during adsorption. The positive values of ΔH^0 (126.42 kJ/mol) suggest that the adsorption of Cd²⁺ on MSCB is an endothermic process, meaning that heat is absorbed from the surroundings. This indicates that the adsorption mechanism is predominantly oriented towards chemisorption, involving chemical bonding between Cd²⁺ and the active sites on the MSCB surface [47, 77–79]. Higher temperatures promoted adsorption, which was consistent with the adsorption isotherm in (Table 3).

3.7 Reusability assessment

The regeneration and reusability of adsorbents are crucial factors for their economic viability and practical uses. In this study, three consecutive sorption and desorption cycles were conducted to examine the reusability of MSCB. Fig. S5 illustrates that the removal efficiencies of MSCB for Cd²⁺ ions were effectively restored, with the adsorption efficiency above 80% following three cycles of reuse utilizing HNO₃ (0.1N, 1 h) as eluent [68, 104, 105]. The findings demonstrated that the engineered MSCB exhibited significant reusability and considerable potential for the sustainable elimination of cadmium. The reduction in adsorption effectiveness may result from partial saturation of the surface active sites or depletion of the surface functional groups of MSCB [106]. As a result, MSCB can be repurposed and

recycled for the adsorption of heavy metals, hence improving process efficiency and promoting economic and environmental sustainability.

3.8 Comparison of maximum adsorption capacity of different adsorbents for cadmium removal

The adsorption capacity of biochar materials for Cd²⁺ varies depending on the raw materials and production processes involved. The adsorption performances of various biochars for Cd²⁺ removal are shown in Table 6, and it can be inferred that MSCB exhibits a relatively higher theoretical adsorption capacity for Cd²⁺ compared to other biochars. In this study, RSM was employed to optimize the key parameters influencing biochar adsorption, including pH, cadmium concentration, and contact time. The aim was to identify the optimal combination conditions that enhance the biochar's adsorption performance. On the other hand, alternative adsorbents require more resources and effort for synthesis and modification than MSCB. Therefore, RSM was utilized to adjust the adsorption preparation conditions, leading to improved efficacy of biochar adsorption. Furthermore, the optimal conditions obtained through optimization vary depending on the specific pollutants. This approach helps avoid the issue of using biochar produced under the same conditions for adsorbing and removing different pollutants,

Table 6 Performance comparison of modified sugarcane bagasse biochar with previous studies using different adsorbents for Cd²⁺ removal

Adsorbents	q_m (mg/g)	References
MSCB	16.87	This study
Walnut shell	11.60	[107]
Banana peels	5.91	[108]
Rice husk biochar	17.80	[109]
Switch grass	5.01	[110]
Chicken manure	10.90	[111]
Coconut shell	3.85	[112]
Rice straw	4.64	[113]
Rice straw	9.35	[114]
Oak wood	3.04	[115]
Spent coffee ground	10.42	[116]
CZ31 residues	8.06	[117]
CY04 residues	7.91	[117]

which could result in low adsorption efficiency for specific pollutants. The comparative results demonstrate that MSCB is a competitive choice for treating wastewater containing Cd^{2+} . Its relatively higher adsorption capacity and the ability to optimize adsorption conditions using RSM make it well-suited for Cd^{2+} removal.

4 Conclusion

In this study, modified biochar (MSCB) was prepared from sugarcane bagasse activated by $\text{Al}(\text{OH})_3$ and efficiently applied to adsorb Cd^{2+} in the aqueous solution. The characterization demonstrated that MSCB presented a higher specific surface area, pore volume, and more functional groups than non-modified bagasse, intimately associated with promoting its adsorption efficiency. Box-Behnken-based RSM model showed optimized process conditions including cadmium concentration, time, and pH which were 20 mg/L, 60 min, and 8, respectively. The results obtained from the RSM could help to run the experimental practices which reduces time and developmental cost. The presently used model has illustrated good agreement of predicted value with the experimental value, indicating the model was highly significant. The pseudo-second-order kinetic model and Langmuir isotherm model fitted the obtained kinetic and isotherm data well, suggesting that Cd^{2+} adsorption onto MSCB was a monolayer and chemical process. Furthermore, MSCB performed well under reusability after three adsorption–desorption experiments. Overall, this work confirms that MSCB can be considered ideal adsorbents for Cd^{2+} removal from wastewater. Future studies should investigate the application of MSCB for contaminated wastewater treatment in pilot and industrial scale, optimize the operational process parameters, and increase the product's recycling rate.

Supplementary Information The online version contains supplementary material available at <https://doi.org/10.1007/s13399-025-06594-6>.

Acknowledgements The authors would like to thank Damietta University, Egypt, and the central laboratory, Faculty of Technology and Development, Zagazig University, for technical support.

Author contribution Mahmoud M. A. Bakr: conceptualization, investigation, methodology, formal analysis, writing — review and editing. Yongtai Wang: investigation, methodology, and formal analysis. Peng Hao: investigation, methodology, and formal analysis. M. M. A. Dawoud: methodology, formal analysis, and validation. Liangcai Peng: conceptualization, writing — review and editing, funding acquisition, and supervision. Yanting Wang: validation, data curation, visualization, and writing — review and editing.

Funding This work was in part supported by the National Natural Science Foundation of China (32470273, 32170268, and 32101701), the National 111 Project of the Ministry of Education of China

(BP0820035 and D17009), and the Initiative Grant of Hubei University of Technology for High-level Talents (GCC20230001).

Data availability All the data generated or analyzed during this study are included in this article.

Declarations

Ethics approval Not applicable.

Consent for publication All the authors agreed to submit this research work for publication.

Competing interests The authors declare no competing interests.

References

- Singh S, Kumar V, Anil AG et al (2021) Adsorption and detoxification of pharmaceutical compounds from wastewater using nanomaterials: a review on mechanism, kinetics, valorization and circular economy. *J Environ Manage* 300:113569. <https://doi.org/10.1016/J.JENVMAN.2021.113569>
- Abu-Danso E, Peräniemi S, Leiviskä T, Bhatnagar A (2018) Synthesis of S-ligand tethered cellulose nanofibers for efficient removal of Pb(II) and Cd(II) ions from synthetic and industrial wastewater. *Environ Pollut* 242:1988–1997. <https://doi.org/10.1016/J.ENVPOL.2018.07.044>
- Ebaid R, Elhussainy E, El-Shourbagy S et al (2017) Protective effect of *Arthrospira platensis* against liver injury induced by copper nanoparticles. *Orient Pharm Exp Med* 17:203–210. <https://doi.org/10.1007/S13596-017-0264-Z/FIGURES/4>
- Kaba P, Shushi S, Gyimah E, et al (2023) Multivariate analysis of heavy metals and human health risk implications associated with fish consumption from the Yangtze river in Zhenjiang City, China. *Water* 15:1999. <https://doi.org/10.3390/W15111999>
- Yang D, Wang L, Li Z et al (2020) Simultaneous adsorption of Cd(II) and As(III) by a novel biochar-supported nanoscale zero-valent iron in aqueous systems. *Sci Total Environ* 708:134823. <https://doi.org/10.1016/J.SCITOTENV.2019.134823>
- Singh S, Kumar Naik TSS, Anil AG et al (2022) Micro (nano) plastics in wastewater: a critical review on toxicity risk assessment, behaviour, environmental impact and challenges. *Chemosphere* 290:133169. <https://doi.org/10.1016/J.CHEMOSPHERE.2021.133169>
- Liu T, Lawluy Y, Shi Y et al (2022) Adsorption of cadmium and lead from aqueous solution using modified biochar: a review. *J Environ Chem Eng* 10:106502. <https://doi.org/10.1016/J.JECE.2021.106502>
- Varmazyari A, Taghizadehghalehjoughi A, Sevim C et al (2020) Cadmium sulfide-induced toxicity in the cortex and cerebellum: in vitro and in vivo studies. *Toxicol Reports* 7:637–648. <https://doi.org/10.1016/J.TOXREP.2020.04.011>
- Zhang W, Zhao Y, Xu Z et al (2020) Morphological and physiological changes of *Broussonetia papyrifera* seedlings in cadmium contaminated soil. *Plants* 9:1–17. <https://doi.org/10.3390/plants9121698>
- Shao W, Ebaid R, Abomohra AEF, Shahan M (2018) Enhancement of Spirulina biomass production and cadmium biosorption using combined static magnetic field. *Bioresour Technol* 265:163–169. <https://doi.org/10.1016/J.BIORTECH.2018.06.009>
- Wu X, Probst A (2021) Influence of ponds on hazardous metal distribution in sediments at a catchment scale (agricultural

- critical zone, S-W France). *J Hazard Mater* 411:125077. <https://doi.org/10.1016/J.JHAZMAT.2021.125077>
12. Haider FU, Liqun C, Coulter JA et al (2021) Cadmium toxicity in plants: impacts and remediation strategies. *Ecotoxicol Environ Saf* 211:111887. <https://doi.org/10.1016/J.ECOENV.2020.111887>
 13. Ge J, Zhang C, Sun YC et al (2019) Cadmium exposure triggers mitochondrial dysfunction and oxidative stress in chicken (*Gallus gallus*) kidney via mitochondrial UPR inhibition and Nrf2-mediated antioxidant defense activation. *Sci Total Environ* 689:1160–1171. <https://doi.org/10.1016/J.SCITOTENV.2019.06.405>
 14. Jing F, Chen C, Chen X et al (2020) Effects of wheat straw derived biochar on cadmium availability in a paddy soil and its accumulation in rice. *Environ Pollut* 257:113592. <https://doi.org/10.1016/J.ENVPOL.2019.113592>
 15. Palansooriya KN, Yang Y, Tsang YF et al (2020) Occurrence of contaminants in drinking water sources and the potential of biochar for water quality improvement: a review. *Crit Rev Environ Sci Technol* 50:549–611. <https://doi.org/10.1080/10643389.2019.1629803>
 16. Wu J, Li Z, Huang D et al (2020) A novel calcium-based magnetic biochar is effective in stabilization of arsenic and cadmium co-contamination in aerobic soils. *J Hazard Mater* 387:122010. <https://doi.org/10.1016/J.JHAZMAT.2019.122010>
 17. Zhang H, Reynolds M (2019) Cadmium exposure in living organisms: a short review. *Sci Total Environ* 678:761–767. <https://doi.org/10.1016/J.SCITOTENV.2019.04.395>
 18. Abomohra AEF, El-Hefnawy ME, Wang Q et al (2021) Sequential bioethanol and biogas production coupled with heavy metal removal using dry seaweeds: towards enhanced economic feasibility. *J Clean Prod* 316:128341. <https://doi.org/10.1016/J.JCLEPRO.2021.128341>
 19. Ahmad A, Khan N, Giri BS et al (2020) Removal of methylene blue dye using rice husk, cow dung and sludge biochar: characterization, application, and kinetic studies. *Bioresour Technol* 306:123202. <https://doi.org/10.1016/J.BIORTECH.2020.123202>
 20. Szczepański P, Guo H, Dzieszowski K et al (2021) New reactive ionic liquids as carriers in polymer inclusion membranes for transport and separation of Cd(II), Cu(II), Pb(II), and Zn(II) ions from chloride aqueous solutions. *J Memb Sci* 638:119674. <https://doi.org/10.1016/J.MEMSCI.2021.119674>
 21. Wang X, Cai D, Ji M et al (2022) Isolation of heavy metal-immobilizing and plant growth-promoting bacteria and their potential in reducing Cd and Pb uptake in water spinach. *Sci Total Environ* 819:153242. <https://doi.org/10.1016/J.SCITOTENV.2022.153242>
 22. Jlassi K, Eid K, Sliem MH et al (2020) Calix[4]arene-clicked clay through thiol-yne addition for the molecular recognition and removal of Cd(II) from wastewater. *Sep Purif Technol* 251:117383. <https://doi.org/10.1016/J.SEPPUR.2020.117383>
 23. Xu S, Liu Y, Yu Y et al (2020) PAN/PVDF chelating membrane for simultaneous removal of heavy metal and organic pollutants from mimic industrial wastewater. *Sep Purif Technol* 235:116185. <https://doi.org/10.1016/J.SEPPUR.2019.116185>
 24. Esfahani AR, Zhai L, Sadmani AHMA (2021) Removing heavy metals from landfill leachate using electrospun polyelectrolyte fiber mat-laminated ultrafiltration membrane. *J Environ Chem Eng* 9:105355. <https://doi.org/10.1016/j.jece.2021.105355>
 25. Deng Y, Huang S, Dong C et al (2020) Competitive adsorption behaviour and mechanisms of cadmium, nickel and ammonium from aqueous solution by fresh and ageing rice straw biochars. *Bioresour Technol* 303:122853. <https://doi.org/10.1016/J.BIORTECH.2020.122853>
 26. Yin K, Wang J, Zhai S et al (2022) Adsorption mechanisms for cadmium from aqueous solutions by oxidant-modified biochar derived from *Platanus orientalis* Linn leaves. *J Hazard Mater* 428:128261. <https://doi.org/10.1016/J.JHAZMAT.2022.128261>
 27. Zhang Z, Li Y, Ding L et al (2021) Novel sodium bicarbonate activation of cassava ethanol sludge derived biochar for removing tetracycline from aqueous solution: performance assessment and mechanism insight. *Bioresour Technol* 330:124949. <https://doi.org/10.1016/J.BIORTECH.2021.124949>
 28. Kaur M, Tewatia P, Rattan G et al (2021) Diamidoximated cellulosic bioadsorbents from hemp stalks for elimination of uranium (VI) and textile waste in aqueous systems. *J Hazard Mater* 417:126060. <https://doi.org/10.1016/J.JHAZMAT.2021.126060>
 29. Jiang D, Li H, Cheng X et al (2023) A mechanism study of methylene blue adsorption on seaweed biomass derived carbon: from macroscopic to microscopic scale. *Process Saf Environ Prot* 172:1132–1143. <https://doi.org/10.1016/J.PSEP.2023.02.044>
 30. Madadi M, Bakr MM, Song G et al (2022) Co-production of levulinic acid and lignin adsorbent from aspen wood with combination of liquid hot water and green-liquor pretreatment. *Elsevier J Clean Prod* 366:132817. <https://doi.org/10.1016/j.jclepro.2022.132817>
 31. Xiao J, Hu R, Chen G (2020) Micro-nano-engineered nitrogenous bone biochar developed with a ball-milling technique for high-efficiency removal of aquatic Cd(II), Cu(II) and Pb(II). *J Hazard Mater* 387:121980. <https://doi.org/10.1016/J.JHAZMAT.2019.121980>
 32. Pap S, Bezanovic V, Radonic J et al (2018) Synthesis of highly-efficient functionalized biochars from fruit industry waste biomass for the removal of chromium and lead. *J Mol Liq* 268:315–325. <https://doi.org/10.1016/J.MOLLIQ.2018.07.072>
 33. Berslin D, Reshmi A, Sivaprakash B et al (2022) Remediation of emerging metal pollutants using environment friendly biochar- review on applications and mechanism. *Chemosphere* 290:133384. <https://doi.org/10.1016/J.CHEMOSPHERE.2021.133384>
 34. Gong H, Tan Z, Huang K et al (2021) Mechanism of cadmium removal from soil by silicate composite biochar and its recycling. *J Hazard Mater* 409:125022. <https://doi.org/10.1016/J.JHAZMAT.2020.125022>
 35. Shen W, Cao B, Mu M et al (2023) Monophenols recovery by catalytic pyrolysis of waste sawdust over activated biochar from the brown macroalgae *Hizikia fusiformis*: Mechanism and life-cycle assessment. *J Anal Appl Pyrolysis* 169:105798. <https://doi.org/10.1016/J.JAAP.2022.105798>
 36. Nie T, Yang X, Chen H et al (2021) Effect of biochar aging and co-existence of diethyl phthalate on the mono-sorption of cadmium and zinc to biochar-treated soils. *J Hazard Mater* 408:124850. <https://doi.org/10.1016/J.JHAZMAT.2020.124850>
 37. Wen E, Yang X, Chen H et al (2021) Iron-modified biochar and water management regime-induced changes in plant growth, enzyme activities, and phytoavailability of arsenic, cadmium and lead in a paddy soil. *J Hazard Mater* 407:124344. <https://doi.org/10.1016/J.JHAZMAT.2020.124344>
 38. Wang B, Gao B, Fang J (2017) Recent advances in engineered biochar productions and applications. *Crit Rev Environ Sci Technol* 47:2158–2207. <https://doi.org/10.1080/10643389.2017.1418580>
 39. Premarathna KSD, Rajapaksha AU, Sarkar B et al (2019) Biochar-based engineered composites for sorptive decontamination of water: a review. *Chem Eng J* 372:536–550. <https://doi.org/10.1016/J.CEJ.2019.04.097>
 40. Wu B, Wan J, Zhang Y et al (2020) Selective phosphate removal from water and wastewater using sorption: process fundamentals and removal mechanisms. *Environ Sci Technol* 54:50–66. https://doi.org/10.1021/ACS.EST.9B05569/ASSET/IMAGES/LARGE/ES9B05569_0004.JPEG

41. Chen M, He F, Hu D et al (2020) Broadened operating pH range for adsorption/reduction of aqueous Cr(VI) using biochar from directly treated jute (*Corchorus capsularis* L.) fibers by H3PO4. *Chem Eng J* 381:122739. <https://doi.org/10.1016/J.CEJ.2019.122739>
42. An Q, Jiang YQ, Nan HY et al (2019) Unraveling sorption of nickel from aqueous solution by KMnO4 and KOH-modified peanut shell biochar: implicit mechanism. *Chemosphere* 214:846–854. <https://doi.org/10.1016/J.CHEMOSPHERE.2018.10.007>
43. Yuan P, Fan M, Yang D et al (2009) Montmorillonite-supported magnetite nanoparticles for the removal of hexavalent chromium [Cr(VI)] from aqueous solutions. *J Hazard Mater* 166:821–829. <https://doi.org/10.1016/J.JHAZMAT.2008.11.083>
44. Popat KM, Anand PS, Dasare BD (1994) Selective removal of fluoride ions from water by the aluminium form of the amino-methylphosphonic acid-type ion exchanger. *React Polym* 23:23–32. [https://doi.org/10.1016/0923-1137\(94\)90107-4](https://doi.org/10.1016/0923-1137(94)90107-4)
45. Piñón-Miramontes M, Fluoride RB-M-, 2003] undefined (2003) Removal of arsenic and fluoride from drinking water with cake alum and a polymeric anionic flocculent. *Fluoride* 36:122–128
46. Nguyen TH, Nguyen TTL, Nguyen TC et al (2023) Adsorption behavior of cationic surfactant onto aluminum hydroxide nanoparticles and application in lindane removal. *Mater Today Commun* 34:105266. <https://doi.org/10.1016/J.MTCOMM.2022.105266>
47. Franks GV, Gan Y (2007) Charging behavior at the alumina–water interface and implications for ceramic processing. *J Am Ceram Soc* 90:3373–3388. <https://doi.org/10.1111/J.1551-2916.2007.02013.X>
48. He P, Zou Y, Hu Z (2015) Advances in aluminum hydroxide-based adjuvant research and its mechanism. *Hum Vaccin Immunother* 11:477–488. <https://doi.org/10.1080/21645515.2014.1004026>
49. Pan M, Lin X, Xie J, Huang X (2017) Kinetic, equilibrium and thermodynamic studies for phosphate adsorption on aluminum hydroxide modified palygorskite nano-composites. *RSC Adv* 7:4492–4500. <https://doi.org/10.1039/C6RA26802A>
50. Lozhkomoev AS, Lerner MI, Tsukanov AA et al (2017) On the possibility of soft matter nanostructure formation based on mesoporous aluminum hydroxide. *Prospects Biomed Appl Phys Mesomech* 20:134–141. <https://doi.org/10.1134/S1029959917020035/METRICS>
51. Xu R, Zhang M, Mortimer RJG, Pan G (2017) Enhanced phosphorus locking by novel lanthanum/aluminum-hydroxide composite: implications for eutrophication control. *Environ Sci Technol* 51:3418–3425. https://doi.org/10.1021/ACS.EST.6B05623/SUPPL_FILE/ES6B05623_SI_001.PDF
52. Heidari N, Momeni P (2017) Selective adsorption of lithium ions from Urmia Lake onto aluminum hydroxide. *Environ Earth Sci* 76:1–8. <https://doi.org/10.1007/S12665-017-6885-1/TABLES/7>
53. Lee HS, Shin HS (2021) Competitive adsorption of heavy metals onto modified biochars: comparison of biochar properties and modification methods. *J Environ Manage* 299:113651. <https://doi.org/10.1016/J.JENVMAN.2021.113651>
54. Niazi NK, Bibi I, Shahid M et al (2018) Arsenic removal by perilla leaf biochar in aqueous solutions and groundwater: an integrated spectroscopic and microscopic examination. *Environ Pollut* 232:31–41. <https://doi.org/10.1016/J.ENVPOL.2017.09.051>
55. Mokhena T, Mochane M, TM S (2018) Sugarcane bagasse and cellulose polymer composites. *Sugarcane-Technol Res p 225*. <https://doi.org/10.5772/intechopen.71497>
56. Van Tran T, Bui QTP, Nguyen TD et al (2017) A comparative study on the removal efficiency of metal ions (Cu²⁺, Ni²⁺, and Pb²⁺) using sugarcane bagasse-derived ZnCl₂-activated carbon by the response surface methodology. *Adsorpt Sci Technol* 35:72–85. <https://doi.org/10.1177/0263617416669152>
57. Kamboj A, Sadh PK, Yadav B et al (2024) Unravelling the potential of sugarcane bagasse: an eco-friendly and inexpensive agro-industrial waste for the production of valuable products using pretreatment processes for sustainable bio-economy. *J Environ Chem Eng* 12:114461. <https://doi.org/10.1016/J.JECE.2024.114461>
58. Iwuozor KO, Chizitere Emenike E, Ighalo JO et al (2022) A review on the thermochemical conversion of sugarcane bagasse into biochar. *Clean Mater* 6:100162. <https://doi.org/10.1016/J.CLEMA.2022.100162>
59. Aruna BN, Sharma AK, Kumar S (2021) A review on modified sugarcane bagasse biosorbent for removal of dyes. *Chemosphere* 268:129309. <https://doi.org/10.1016/J.CHEMOSPHERE.2020.129309>
60. Baharudin IS, Noor NM, Abdullah EC et al (2022) Magnetically modified sugarcane bagasse biochar as cadmium removal agent in water. *IJUM Eng J* 23:294–309. <https://doi.org/10.31436/IJUM.EJ.V23I1.1816>
61. Carolino JM, Braz GS, de Carmo Lima Carvalho J et al (2025) Assessment of the ecotoxicity of extracts from sugarcane bagasse biochars activated with zinc chloride. *Environ Chem Ecotoxicol* 7:19–26. <https://doi.org/10.1016/J.ENCECO.2024.10.002>
62. Pallavi P, Manikandan SK, Nair V (2024) Optimization and mechanistic study on bioremediation of Cr (VI) using microbial cell immobilized sugarcane bagasse biochar. *J Water Process Eng* 58:104859. <https://doi.org/10.1016/J.JWPE.2024.104859>
63. Karimifard S, Alavi Moghaddam MR (2018) Application of response surface methodology in physicochemical removal of dyes from wastewater: a critical review. *Sci Total Environ* 640–641:772–797. <https://doi.org/10.1016/J.SCITOTENV.2018.05.355>
64. Mäkelä M (2017) Experimental design and response surface methodology in energy applications: a tutorial review. *Energy Convers Manag* 151:630–640. <https://doi.org/10.1016/J.ENCONMAN.2017.09.021>
65. Ghaleb AAS, Kutty SRM, Ho YC et al (2020) Response surface methodology to optimize methane production from mesophilic anaerobic co-digestion of oily-biological sludge and sugarcane bagasse. *Sustain* 12:2116. <https://doi.org/10.3390/SU12052116>
66. Lye HL, Mohammed BS, Liew MS et al (2020) Bond behaviour of CFRP-strengthened ECC using response surface methodology (RSM). *Case Stud Constr Mater* 12:e00327. <https://doi.org/10.1016/J.CSCM.2019.E00327>
67. Karacan F, Ozden U, Karacan S (2007) Optimization of manufacturing conditions for activated carbon from Turkish lignite by chemical activation using response surface methodology. *Appl Therm Eng* 27:1212–1218. <https://doi.org/10.1016/J.APPLTHERMALENG.2006.02.046>
68. Isaac R, Siddiqui S, Aldosari OF, Kashif Uddin M (2023) Magnetic biochar derived from *Juglans regia* for the adsorption of Cu²⁺ and Ni²⁺: characterization, modelling, optimization, and cost analysis. *J Saudi Chem Soc* 27:101749. <https://doi.org/10.1016/J.JSCS.2023.101749>
69. Uddin MK, Rao RAK, Chandra Mouli KVV (2018) The artificial neural network and Box-Behnken design for Cu²⁺ removal by the pottery sludge from water samples: equilibrium, kinetic and thermodynamic studies. *J Mol Liq* 266:617–627. <https://doi.org/10.1016/J.MOLLIQ.2018.06.098>
70. White PM, Potter TL, Lima IM (2015) Sugarcane and pinewood biochar effects on activity and aerobic soil dissipation of metribuzin and pendimethalin. *Ind Crops Prod* 74:737–744. <https://doi.org/10.1016/J.INDCROP.2015.04.022>

71. Munim SA, Saddique MT, Raza ZA, Majeed MI (2018) Preparation and physico-chemical characterization of β -cyclodextrin incorporated chitosan biosorbent beads with potential environmental applications. *Mater Res Express* 5:065503. <https://doi.org/10.1088/2053-1591/AAC707>
72. Ayub A, Raza ZA, Majeed MI et al (2020) Development of sustainable magnetic chitosan biosorbent beads for kinetic remediation of arsenic contaminated water. *Int J Biol Macromol* 163:603–617. <https://doi.org/10.1016/j.IJBIOMAC.2020.06.287>
73. Qu J, Li Y, Bi F et al (2024) Smooth vetch (*Vicia villosa* var.) coupled with ball-milled composite mineral derived from shell powder and phosphate rock for remediation of cadmium-polluted farmland: insights into synergetic mechanisms. *ACS ES T Eng* 4:2054–2067. https://doi.org/10.1021/ACSESTENGG.4C00177/ASSET/IMAGES/LARGE/EE4C00177_0009.JPEG
74. Jais F, Chee C, Ismail Z et al (2021) Experimental design via NaOH activation process and statistical analysis for activated sugarcane bagasse hydrochar for removal of dye and antibiotic. *J Environ Chem Eng* 9:104829. <https://doi.org/10.1016/j.jece.2020.104829>
75. Rajapaksha AU, Chen SS, Tsang DCW et al (2016) Engineered/designer biochar for contaminant removal/immobilization from soil and water: potential and implication of biochar modification. *Chemosphere* 148:276–291. <https://doi.org/10.1016/j.CHEMOSPHERE.2016.01.043>
76. Masoumi S, Dalai AK (2020) Optimized production and characterization of highly porous activated carbon from algal-derived hydrochar. *J Clean Prod* 263:121427. <https://doi.org/10.1016/j.JCLEPRO.2020.121427>
77. de Araújo TP, Quesada HB, Bergamasco R et al (2020) Activated hydrochar produced from brewer's spent grain and its application in the removal of acetaminophen. *Bioresour Technol* 310:123399. <https://doi.org/10.1016/j.BIORTECH.2020.123399>
78. Hong SH, Lyonga FN, Kang JK et al (2020) Synthesis of Fe-impregnated biochar from food waste for selenium(VI) removal from aqueous solution through adsorption: process optimization and assessment. *Chemosphere* 252:126475. <https://doi.org/10.1016/j.CHEMOSPHERE.2020.126475>
79. Vyavahare GD, Gurav RG, Jadhav PP et al (2018) Response surface methodology optimization for sorption of malachite green dye on sugarcane bagasse biochar and evaluating the residual dye for phyto and cytogenotoxicity. *Chemosphere* 194:306–315. <https://doi.org/10.1016/j.CHEMOSPHERE.2017.11.180>
80. Zhou R, Zhang M, Li J, Zhao W (2020) Optimization of preparation conditions for biochar derived from water hyacinth by using response surface methodology (RSM) and its application in Pb^{2+} removal. *J Environ Chem Eng* 8:104198. <https://doi.org/10.1016/j.JECE.2020.104198>
81. Islam MA, Ahmed MJ, Khanday WA et al (2017) Mesoporous activated coconut shell-derived hydrochar prepared via hydrothermal carbonization-NaOH activation for methylene blue adsorption. *J Environ Manage* 203:237–244. <https://doi.org/10.1016/j.JENVMAN.2017.07.029>
82. Ghanim B, O'Dwyer TF, Leahy JJ et al (2020) Application of KOH modified seaweed hydrochar as a biosorbent of vanadium from aqueous solution: characterisations, mechanisms and regeneration capacity. *J Environ Chem Eng* 8:104176. <https://doi.org/10.1016/j.JECE.2020.104176>
83. Khanday WA, Majid SA, Chandra Shekar S, Tomar R (2013) Synthesis and characterization of various zeolites and study of dynamic adsorption of dimethyl methyl phosphate over them. *Mater Res Bull* 48:4679–4686. <https://doi.org/10.1016/j.MATER RESBULL.2013.08.003>
84. Khanday WA, Majid SA, Chandra Shekar S, Tomar R (2014) Dynamic adsorption of DMMP over synthetic zeolite-Alpha. *Arab J Chem* 7:115–123. <https://doi.org/10.1016/J.ARABJC.2013.06.026>
85. Hu C, Feng J, Zhou N et al (2021) Hydrochar from corn stalk used as bio-asphalt modifier: High-temperature performance improvement. *Environ Res* 193:110157. <https://doi.org/10.1016/J.ENVRES.2020.110157>
86. Dalali N, Hagghi A (2016) Removal of cadmium from aqueous solutions by walnut green husk as a low-cost biosorbent. *Desalin Water Treat* 57:13782–13794. <https://doi.org/10.1080/19443994.2015.1061952>
87. Sahu MK, Mandal S, Yadav LS et al (2016) Equilibrium and kinetic studies of Cd(II) ion adsorption from aqueous solution by activated red mud. *Desalin Water Treat* 57:14251–14265. <https://doi.org/10.1080/19443994.2015.1062428>
88. Meng K, Wu X, Zhang X et al (2019) Efficient adsorption of the Cd(II) and As(V) Using novel adsorbent ferrihydrite/manganese dioxide composites. *ACS Omega* 4:18627. <https://doi.org/10.1021/ACSOMEGA.9B02431>
89. Mohamed HS, Soliman NK, Abdelrheem DA et al (2019) Adsorption of Cd²⁺ and Cr³⁺ ions from aqueous solutions by using residue of *Padina gymnospora* waste as promising low-cost adsorbent. *Heliyon* 5:e01287. <https://doi.org/10.1016/J.HELIIYON.2019.E01287>
90. Zhang M, Yin Q, Ji X et al (2020) High and fast adsorption of Cd(II) and Pb(II) ions from aqueous solutions by a waste biomass based hydrogel. *Sci Reports* 10(10):1–13. <https://doi.org/10.1038/s41598-020-60160-w>
91. Jiang L, Chen Y, Wang Y et al (2022) Contributions of various Cd(II) adsorption mechanisms by phragmites australis-activated carbon modified with mannitol. *ACS Omega* 7:10502–10515. https://doi.org/10.1021/ACSOMEGA.2C00014/ASSET/IMAGES/LARGE/AO2C00014_0008.JPEG
92. Javadian H, Ghorbani F, Tayebi HA, Asl SMH (2015) Study of the adsorption of Cd (II) from aqueous solution using zeolite-based geopolymer, synthesized from coal fly ash; kinetic, isotherm and thermodynamic studies. *Arab J Chem* 8:837–849. <https://doi.org/10.1016/J.ARABJC.2013.02.018>
93. Silas TV (2017) Characterization and adsorption isotherm studies of Cd (II) and Pb (II) ions bioremediation from aqueous solution using unmodified sorghum husk. *J appl biotechnol bioeng* 2(3):113–120. <https://doi.org/10.15406/JABB.2017.02.00034>
94. Liu F, Zhou K, Chen Q et al (2018) Comparative study on the synthesis of magnetic ferrite adsorbent for the removal of Cd(II) from wastewater. *Adsorpt Sci Technol* 36:1456–1469. <https://doi.org/10.1177/0263617418779729>
95. Mohamed HS, Soliman NK, Abdelrheem DA et al (2019) Adsorption of Cd²⁺ and Cr³⁺ ions from aqueous solutions by using residue of *Padina gymnospora* waste as promising low-cost adsorbent. *Heliyon* 5(3):1–13. <https://doi.org/10.1016/J.HELIIYON.2019.E01287>
96. Lei T, Li SJ, Jiang F et al (2019) Adsorption of cadmium ions from an aqueous solution on a highly stable dopamine-modified magnetic nano-adsorbent. *Nanoscale Res Lett* 14:1–17. <https://doi.org/10.1186/S11671-019-3154-0/FIGURES/7>
97. Es-said A, Nafai H, Lamzougui G et al (2021) Comparative adsorption studies of cadmium ions on phosphogypsum and natural clay. *Sci African* 13:e00960. <https://doi.org/10.1016/J.SCIAF.2021.E00960>
98. Ofgea NM, Tura AM, Fanta GM (2022) Activated carbon from H₃PO₄-activated *Moringa stenopetale* seed husk for removal of methylene blue: optimization using the response surface method (RSM). *Environ Sustain Indic* 16:100214. <https://doi.org/10.1016/J.INDIC.2022.100214>

99. Lopez-Ramon MV, Stoeckli F, Moreno-Castilla C, Carrasco-Marin F (1999) On the characterization of acidic and basic surface sites on carbons by various techniques. *Carbon* N Y 37:1215–1221. [https://doi.org/10.1016/S0008-6223\(98\)00317-0](https://doi.org/10.1016/S0008-6223(98)00317-0)
100. Danish M, Ahmad T, Hashim R et al (2018) Comparison of surface properties of wood biomass activated carbons and their application against rhodamine B and methylene blue dye. *Surf Interfaces* 11:1–13. <https://doi.org/10.1016/J.SURFIN.2018.02.001>
101. Liu L, Luo XB, Ding L, Luo SL (2019) Application of nanotechnology in the removal of heavy metal from water. *Nanomaterials for the removal of pollutants and resource reutilization* Elsevier, pp 83–147. <https://doi.org/10.1016/B978-0-12-814837-2.00004-4>
102. Rai P, Preeti S et al (2022) Sequestration of cadmium ions from aqueous phase using magnetic chitosan composite. *Mater Today Proc* 49:3375–3383. <https://doi.org/10.1016/J.MATPR.2021.01.845>
103. Ezeonuegbu BA, Machido DA, Whong CMZ et al (2021) Agricultural waste of sugarcane bagasse as efficient adsorbent for lead and nickel removal from untreated wastewater: biosorption, equilibrium isotherms, kinetics and desorption studies. *Biotechnol Reports* 30:e00614. <https://doi.org/10.1016/J.BTRE.2021.E00614>
104. Sulaiman MS, Ajayi OA, Olakunle MS (2024) Optimization of cadmium adsorption on metal organic frameworks MIL-53(Fe) using response surface methodology. *Inorg Chem Commun* 159:111765. <https://doi.org/10.1016/J.INOCHE.2023.111765>
105. Patel H (2021) Review on solvent desorption study from exhausted adsorbent. *J Saudi Chem Soc* 25:101302. <https://doi.org/10.1016/J.JSCS.2021.101302>
106. Zhang L, Ren Y, Xue Y et al (2020) Preparation of biochar by mango peel and its adsorption characteristics of Cd(II) in solution. *RSC Adv* 10:35878–35888. <https://doi.org/10.1039/D0RA06586B>
107. Almasi A, Omid M, Khodadadian M et al (2012) Lead(II) and cadmium(II) removal from aqueous solution using processed walnut shell: kinetic and equilibrium study. *Toxicol Environ Chem* 94:660–671. <https://doi.org/10.1080/02772248.2012.671328>
108. Deshmukh PD, Khadse GK, Shinde VM, Labhasetwar P (2017) Cadmium removal from aqueous solutions using dried banana peels as an adsorbent: kinetics and equilibrium modeling. *J Bioremediat Biodegrad* 8(03):1–7. <https://doi.org/10.4172/2155-6199.1000395>
109. Ameen Hezam Saeed A, Yub Harun N, Mahmoud Nasef M et al (2022) Removal of cadmium from aqueous solution by optimized rice husk biochar using response surface methodology. *Ain Shams Eng J* 13(1):101516. <https://doi.org/10.1016/j.asej.2021.06.002>
110. Sardella F, Gimenez M, Navas C et al (2015) Conversion of viticultural industry wastes into activated carbons for removal of lead and cadmium. *J Environ Chem Eng* 3:253–260. <https://doi.org/10.1016/J.JECE.2014.06.026>
111. Higashikawa FS, Conz RF, Colzato M et al (2016) Effects of feedstock type and slow pyrolysis temperature in the production of biochars on the removal of cadmium and nickel from water. *J Clean Prod* 137:965–972. <https://doi.org/10.1016/J.JCLEPRO.2016.07.205>
112. Yap MW, Mubarak NM, Sahu JN, Abdullah EC (2017) Microwave induced synthesis of magnetic biochar from agricultural biomass for removal of lead and cadmium from wastewater. *J Ind Eng Chem* 45:287–295. <https://doi.org/10.1016/J.JIEC.2016.09.036>
113. Huang F, Zhang SM, Wu RR et al (2021) Magnetic biochars have lower adsorption but higher separation effectiveness for Cd²⁺ from aqueous solution compared to nonmagnetic biochars. *Environ Pollut* 275:116485. <https://doi.org/10.1016/J.ENVPOL.2021.116485>
114. Wang YP, Liu YL, Tian SQ, et al (2021) Straw biochar enhanced removal of heavy metal by ferrate. *J Hazard Mater* 416:126128. <https://doi.org/10.1016/j.jhazmat.2021.126128>
115. Mohan D, Kumar H, Sarswat A et al (2014) Cadmium and lead remediation using magnetic oak wood and oak bark fast pyrolysis bio-chars. *Chem Eng J* 236:513–528. <https://doi.org/10.1016/J.CEJ.2013.09.057>
116. Hussain N, Chantrapromma S, Suwunwong T, Phoungthong K (2020) Cadmium (II) removal from aqueous solution using magnetic spent coffee ground biochar: Kinetics, isotherm and thermodynamic adsorption. *Mater Res Express* 7:085503. *Mater Res Express* 7(8):085503. <https://doi.org/10.1088/2053-1591/ABAE27>
117. Xu C, Xia T, Wang J et al (2021) Selectively desirable rapeseed and corn stalks distinctive for low-cost bioethanol production and high-active biosorbents. *Waste and Biomass Valorization* 12:795–805. <https://doi.org/10.1007/S12649-020-01026-0/TABLES/5>

Publisher's Note Springer Nature remains neutral with regard to jurisdictional claims in published maps and institutional affiliations.

Springer Nature or its licensor (e.g. a society or other partner) holds exclusive rights to this article under a publishing agreement with the author(s) or other rightsholder(s); author self-archiving of the accepted manuscript version of this article is solely governed by the terms of such publishing agreement and applicable law.